Journal of Statistical Physics, Vol. 57, Nos. 3/4, 1989

Scaling Behavior of Two-Dimensional Domain Growth: Computer Simulation of Vertex Models

Katsuya Nakashima,[1] Tatsuzo Nagai,[2] and Kyozi Kawasaki[1]

Received February, 1989

Computer simulations are performed for vertex models which are coarse-grained models for dynamical cellular patterns in two dimensions. By simulating large systems, we obtain conclusive evidence of scaling behavior, that is, a power law for the growth of the average cell size and the scaling properties for the distribution functions of edge number and size of cells. Several versions of the vertex models are obtained by making some approximations for the equation of motion of a vertex, and we compare the statistical properties of the patterns in the scaling regime.

KEY WORDS: Domain growth; cellular pattern; scaling behavior; vertex model.

1. INTRODUCTION

We investigate the scaling behavior in two-dimensional domain growth. We consider the coarsening of random cellular systems, such as two-dimensional grain aggregates and two-dimensional soap froths. The method of description and the evolution laws of such dynamical cellular patterns are still poorly understood. Many previous works suggest scaling behavior, that is, such patterns develop in a self-similar way at long times, during which the average cell size grows as a power law in time, the distribution function of cell sizes has the scaling property with the average cell size and the distribution function of the number of edges of a cell independent of time.

[1] Department of Physics, Faculty of Science, Kyushu University 33, Fukuoka 812, Japan.
[2] Department of General Education, Kyushu Kyoritsu University, Kitakyushu 807, Japan.

0022-4715/89/1100-0759$06.00/0

822/57/3-4-22

Many experimental works on grain aggregates have yielded no conclusive evidence for scaling behavior. In those systems, many secondary effects affect the dynamics of cellular patterns and yield a variety of results. On the other hand, recent experiments[1,2] in two-dimensional soap froths have shown definitive evidence of the existence of scaling behavior for the first time.

Although many computer simulations were carried out on the domain growth problem, there was no convincing proof of the scaling behavior. It requires a large enough number of cells and a long enough simulation time to prove definitely the existence of scaling behavior by computer simulation. The extensively studied Potts model[3] and the curvature-driven model[4] are not efficient enough for this purpose, since their simulation models are too detailed and require large computer memory and the long CPU time.

Recently Beenakker has overcome the difficulty mentioned above by reducing the number of variables which describe the cells.[5] He describes a cell in terms of two variables, its area and number of edges. This is a great reduction in the number of variables compared with the detailed models mentioned above. Correlations between neighboring cells are also included. The area of each cell varies according to the von Neumann–Mullins equation. When the area of a cell vanishes, a topological change takes place. This model permitted the computer simulation of large systems (about 10^5 cells initially) with long coarsening times and demonstrated the existence of scaling behavior in a random cellular system.

Beenakker's model, however, is not deterministic, because he invoked a probabilistic method for reconnecting cell edges after the cell annihilation in the elementary process of topological change. This is inevitable, given the lack of information on the edge of each cell in this model. In addition, this lack of information obliged him to neglect the recombination process, the so-called "T1-process," which is another kind of elementary process of topological change. This approximation had an effect on the distribution function of the number of edges of a cell, which largely deviates from the experimental result observed recently in two-dimensional soap froths.[2] As the von Neumann–Mullins equation shows, the number of edges of a cell governs the time evolution of its area. This suggests that the way of reconnecting cell edges in the two elementary processes of topological change plays an essential role in the dynamics of cellular patterns and that it should be determined according to a deterministic rule which takes local environments of individual cells into account.

In the present paper we present details of our computer simulation studies of the scaling behavior of the domain growth comprehensively for the vertex model of two-dimensional domain growth which has been developed recently.[6–9] The vertex model is a corse-grained model of

dynamical cellular patterns in two dimensions which are expressed in terms of the coarse-grained vertices (intersections of cell boundaries) and coarse-grained straight cell boundaries. The coarse graining involves some temporal and spatial averages. Hence this model has poorer temporal and spatial resolutions than the original system and works if we are only interested in the variations of cellular patterns over time and distance scales greater than the resolution of the model. In fact, we are concerned with statistical quantities, such as the distribution functions of the cell area and the number of edges of cells, and with the slow time evolution of cellular patterns. The knowledge of the motion of vertices gives complete knowledge of the motion of a cellular pattern in this model, with a greatly reduced number of variables. Furthermore, this model properly includes the two elementary processes of topological change mentioned above and is completely deterministic. The previous computer simulations for this type of model revealed a square root power law of the average linear size of cells and an indication of the existence of scaling behavior in the vertex model.[6,7] In the present paper, the scaling behavior will be well established and the asymptotic forms of the distribution functions will be determined with a high accuracy by simulating a system which is ten times larger than that of the previous simulations and repeating about 20 runs. Three versions of vertex models also will be compared.

2. VERTEX MODEL

We briefly review the vertex model in this section, which consists of the equations of motion for vertices and the elementary processes for vertex collisions.[9]

If the motion of cell boundaries is purely dissipative, the equation of motion for the ith vertex which has the position $\mathbf{r}_i$ and the velocity $\mathbf{v}_i$ is given by

$$\frac{\partial \mathscr{F}}{\partial \mathbf{r}_i} + \frac{\partial \mathscr{R}}{\partial \mathbf{v}_i} = 0, \qquad i = 1, 2, \ldots, N \tag{2.1}$$

where $\mathscr{F}$ and $\mathscr{R}$ denote the free energy and the Rayleigh dissipation function, respectively, and N is the number of vertices. In systems with an interface, $\mathscr{F}$ and $\mathscr{R}$ can be generally expressed as follows:

$$\begin{aligned} \mathscr{F} &= \sigma \int da \\ \mathscr{R} &= \frac{\sigma}{2L} \int da\, v(a)^2 \end{aligned} \tag{2.2}$$

where σ is the line tension energy, L is the Onsager kinetic coefficient, and $v(a)$ is the velocity of the interface along its normal direction at the position a on the interface. The integrations in Eqs. (2.2) are over all the interfaces. For the vertex model, Eqs. (2.2) become

$$\begin{aligned} \mathscr{F} &= \sigma \sum_{\langle ij \rangle} |\mathbf{r}_{ij}| \\ \mathscr{R} &= \frac{\sigma}{6L}\left[\sum_i \sum_j^{(i)} |\mathbf{r}_{ij}| (\mathbf{v}_i \cdot \mathbf{n}_{ij})^2 + \sum_{\langle ij \rangle} |\mathbf{r}_{ij}| (\mathbf{v}_i \cdot \mathbf{n}_{ij})(\mathbf{v}_j \cdot \mathbf{n}_{ij}) \right] \end{aligned} \tag{2.3}$$

where $\mathbf{r}_{ij} \equiv \mathbf{r}_i - \mathbf{r}_j$ and $\mathbf{n}_{ij}$ is the normal unit vector of the straight cell boundary segment $\langle ij \rangle$. Furthermore, the sum $\sum_{\langle ij \rangle}$ is over all the connected vertex pairs $\langle ij \rangle$ and the sum $\sum_j^{(i)}$ over three vertices j which are connected to the vertex i. From Eqs. (2.1) and (2.3) we obtain the equation of motion for the ith vertex,

$$\sum_j^{(i)} \mathbf{D}_{ij} \left(\mathbf{v}_i + \frac{1}{2} \mathbf{v}_j \right) = - \sum_j^{(i)} \frac{\mathbf{r}_{ij}}{|\mathbf{r}_{ij}|} \tag{2.4}$$

where $\mathbf{D}_{ij}$ is the tensor defined as

$$(D_{ij})^{\alpha\beta} = \frac{1}{3L} |\mathbf{r}_{ij}| \, n_{ij}^{\alpha} n_{ij}^{\beta}, \qquad \alpha, \beta = x, y \tag{2.5}$$

Equation (2.4) describes that the vertex i moves under the action of the resultant of line tensions with $\sigma = 1$ on the rhs in a medium with the friction coefficient $\sum_j^{(i)} \mathbf{D}_{ij}$ if we neglect the term $\mathbf{v}_j/2$ on the lhs. The term $\mathbf{v}_j/2$ gives rise to the correlation of the vertex with its neighbors j and hence will be called the correlation term in the following.

It is expected that the equation of motion for vertex (2.4) approximately describes the grain growth and the evolution of soap froth. The difference of the vertex velocity given by Eq. (2.4) from those in the two cases has been examined in the special case of a symmetric cell having n sides.[9] The discrepancies in the velocities of vertices are within 10% for $n \geqslant 5$, about 25% for $n = 4$, and about 100% for $n = 3$. The large difference for $n = 3$ comes from the difference in the curvature of cell boundaries between the vertex model and the two real systems, which becomes largest for $n = 3$.

Equation (2.4) for the system composed of N vertices constitutes simultaneous equations with $2N$ unknowns for vertex velocities, since the equation for each vertex contains the velocities of its neighbors. It is impractical to solve it directly for large N. We are interested in the behavior of the system at the limit $N \to \infty$. Hence we need to reduce

Eq. (2.4) to a more tractable equation which still retains its essential features.

We neglect all the anisotropy about the vertex i in question on the lhs of Eq. (2.4). That is, we average over all the directions of $\mathbf{n}_{ij}$ and $\mathbf{v}_j$ on the lhs in Eq. (2.4). Then we obtain what we have called the model II equation[9]:

$$\frac{1}{6L}\sum_{j}^{(i)} |\mathbf{r}_{ij}|\, \mathbf{v}_i = -\sum_{j}^{(i)} \frac{\mathbf{r}_{ij}}{|\mathbf{r}_{ij}|} \tag{2.6}$$

This equation shows that the friction coefficient of a vertex is proportional to the sum of distances to its three neighbors and that the velocity of a vertex is not affected by the velocities of its neighbors. If we replace the bond lengths $|\mathbf{r}_{ij}|$ by their average $r_B(t)$ over the system on the lhs in Eq. (2.6), we then obtain what we have called the model I equation[9]:

$$\frac{r_B}{2L}\mathbf{v}_i = -\sum_{j}^{(i)} \frac{\mathbf{r}_{ij}}{|\mathbf{r}_{ij}|} \tag{2.7}$$

Introducing a new time variable τ in place of the physical time variable t according to

$$\tau = \int_0^t \frac{2L}{r_B(s)}\, ds \tag{2.8}$$

we obtain that Eq. (2.7) reduces to

$$\frac{d\mathbf{r}_i}{d\tau} = -\sum_{j}^{(i)} \frac{\mathbf{r}_{ij}}{|\mathbf{r}_{ij}|} \tag{2.9}$$

Equation (2.9) is the simplest version of the vertex equation where the friction coefficient is constant if we regard τ as a new time.

The model equations I and II obtained above both retain the essential features from the viewpoint of dimensional analysis. The differences between the two model equations and the original one (2.4) with respect to topological aspects of the cell pattern will be examined in this paper.

Our model equations of motion must be supplemented with the following two elementary processes of collision, which yield topological changes of the pattern: (i) Recombination process: when two vertices come within the small distance Δ, they are recombined as shown in Fig. 1a, provided that the edge between them belongs to none of the triangular cells. (ii) Triangular annihilation process: when any two of three vertices forming a triangular cell come within the distance Δ, the triangle is transformed into a single vertex at the midpoint between the two vertices as

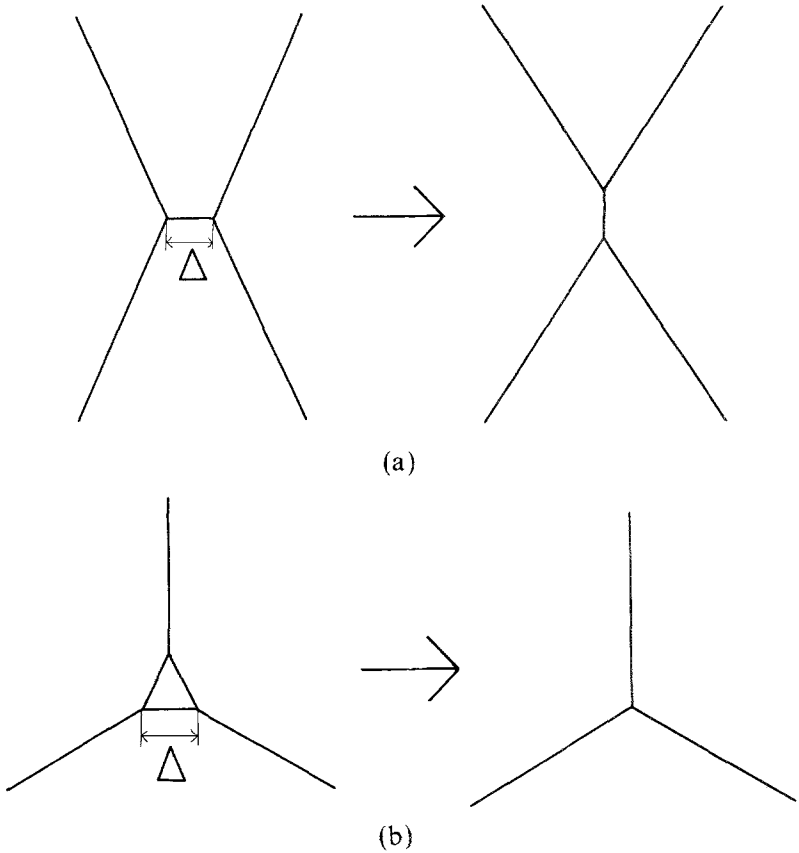

Fig. 1. Elementary collision processes: (a) recombination, (b) triangular annihilation. Δ denotes the vertex size.

shown in Fig. 1b. The length Δ is the spatial resolution in this coarse-grained model and will be called the vertex size.

The above elementary processes are the same as those in soap froths and grain aggregates. They result in changes of the number of edges of cells and in turn affect the time evolution of each cell. Therefore it is important to carry them out precisely in the simulation.

3. SIMULATION METHOD

We carry out computer simulations for the three versions of the vertex model, that is, the simplified models I and II and the original one, and compare their results.

Two kinds of cellular patterns are used for the initial distribution. One is the Voronoi cell network created by using an algorithm described in the Appendix and depicted in Fig. 2a. We choose the Voronoi cell network as the initial configuration to obtain all the simulation data which are analyzed in detail in this paper. Another cellular pattern is constructed as

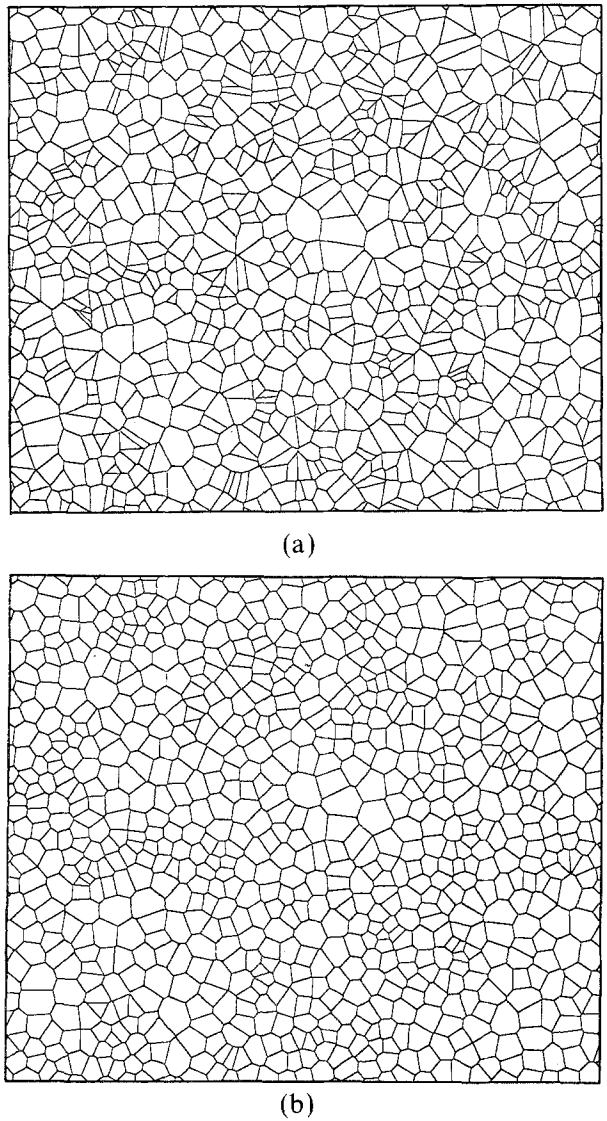

Fig. 2. Initial distributions used in the present simulations: (a) network of the Voronoi cells, (b) pattern created by using the algorithm described in Section 3.

follows: First, create a Voronoi cell network; then determine the center of gravity of each cell; lastly, construct a new cell network regarding those centers of gravity as new nuclei and using the algorithm for the Voronoi cell network. This is different from the first one in regard to nucleus configuration. The resulting pattern is shown in Fig. 2b. It is seen from Figs. 2a and 2b that the latter has more six-sided cells and the sizes of the cells are more homogeneous than the former. We study the latter in order to examine whether or not the late-stage patterns depend on initial configurations.

Initially, the system consists of 48,000 vertices, i.e., 24,000 cells. This number of vertices is ten times as large as those of our previous simulations[6,7] and further 20 runs are carried out. These lead to better statistics and enable us to discuss the distributions of cell sizes and cell edges more definitely.

We choose the quantities $[\bar{A}(0)]^{1/2}$ and $\bar{A}(0)/L$ as the unit of length and the unit of time, respectively, where $\bar{A}(0)$ is the initial average area of a cell. Our system has a rectangular form with a size about 141×170 in the new unit of length and is subjected to periodic boundary condition. We use the same notations $(\mathbf{r}_i, \mathbf{v}_i, t)$ for the dimensionless quantities measured in the new units in this section. Then the model I equations (2.8) and (2.9) become

$$\frac{d\mathbf{r}_i}{d\tau} = -\sum_j^{(i)} \frac{\mathbf{r}_{ij}}{|\mathbf{r}_{ij}|} \tag{3.1}$$

where

$$\tau = 2\int_0^t ds \frac{1}{r_B(s)} \tag{3.2}$$

The model II equation (2.6) is written as

$$\left(\frac{1}{6}\sum_j^{(i)} |\mathbf{r}_{ij}|\right)\frac{d\mathbf{r}_i}{dt} = -\sum_j^{(i)} \frac{\mathbf{r}_{ij}}{|\mathbf{r}_{ij}|} \tag{3.3}$$

Furthermore, the original model equation (2.4) is solved iteratively as follows. If $\mathbf{v}_i^{(0)}$ is assumed to be the solution which satisfies Eq. (2.4) without the correlation term $\frac{1}{2}\mathbf{v}_j$ on the lhs then the solution $\mathbf{v}_i^{(n)}$ obtained after n iterations is determined by

$$\sum_j^{(i)} \mathbf{D}_{ij}\left(\mathbf{v}_i^{(n)} + \frac{1}{2}\mathbf{v}_j^{(n-1)}\right) = -\sum_j^{(i)} \frac{\mathbf{r}_{ij}}{|\mathbf{r}_{ij}|}, \qquad n \geqslant 1 \tag{3.4}$$

where

$$(D_{ij})^{\alpha\beta} = \tfrac{1}{3}|\mathbf{r}_{ij}|\, n_{ij}^{\alpha} n_{ij}^{\beta}, \qquad \alpha, \beta = x, y \tag{3.5}$$

The number n of iterations is taken to be the number which satisfies the following inequality at each time:

$$\max_i \{(\mathbf{v}_i^{(n)} - \mathbf{v}_i^{(n-1)})^2/(\mathbf{v}_i^{(n)})^2\}^{1/2} < 10^{-3} \tag{3.6}$$

We have adopted $n = 20$ in practice. The resulting $\mathbf{v}_i^{(n)}(\{\mathbf{r}_k\})$ can be used to find the following simultaneous differential equation for the original model:

$$\frac{d\mathbf{r}_i}{dt} = \mathbf{v}_i^{(n)}(\{\mathbf{r}_k\}) \tag{3.7}$$

Three sets of simultaneous differential equations (3.1), (3.3), and (3.7) are numerically solved employing the Runge–Kutta–Gill method. The step size in time employed in solving these equations is 0.01. The vertex size Δ is 0.01, 0.1, and 0.2 in model I, model II, and the original model, respectively. These values of the parameters are chosen in such a way that the displacement of any vertex does not exceed Δ in a single time step. Otherwise unphysical processes may occur, such as cell boundary crossing and long-lived oscillation of two vertices which are connected with each other by a short cell boundary whose length is of the order of but longer than Δ. Any value of Δ chosen above is such that it becomes mostly invisible in the patterns in the late stage. It is expected that Δ has no effect on the cell pattern in the late stage if Δ is much smaller than the average cell size.

In practice, we need to introduce another elementary process besides the two elementary processes mentioned in the previous section. It takes place when two neighboring triangles annihilate simultaneously. In this case, we adopt the new process in which the two triangles vanish completely and then the two outer lines become a single line.

4. SCALING BEHAVIOR

We have executed the computer simulation by using the method mentioned in the previous section, and we show typical growing patterns obtained for model II in Fig. 3. These figures show self-similar development of the pattern, and a resemblance of the patterns to those observed in grain aggregates and soap froths in two dimensions. In order to investigate the existence of the scaling behavior in the late stage, we examine the time dependences of the average cell sizes, the distribution function of the number of edges, and the distribution function of the cell size.

First we study the growth law of the cell size. It is commonly accepted that the average cell size $\bar{R}(t)$ grows as $\bar{R} \sim t^{\alpha}$ in the late stage of growth, which is called the scaling regime. If the size distribution of cells has the

scaling property, the square of $\bar{R}(t)$ is proportional to the average cell area $\bar{A}(t)$. Thus, we examine the growth of $\bar{A}(t)$. As we have set the unit of length as $\bar{A}(0)=1$, the average cell area $\bar{A}(t)$ is written in terms of the total number of vertices $N(t)$ as follows:

$$\bar{A}(t)=N(0)/N(t) \tag{4.1}$$

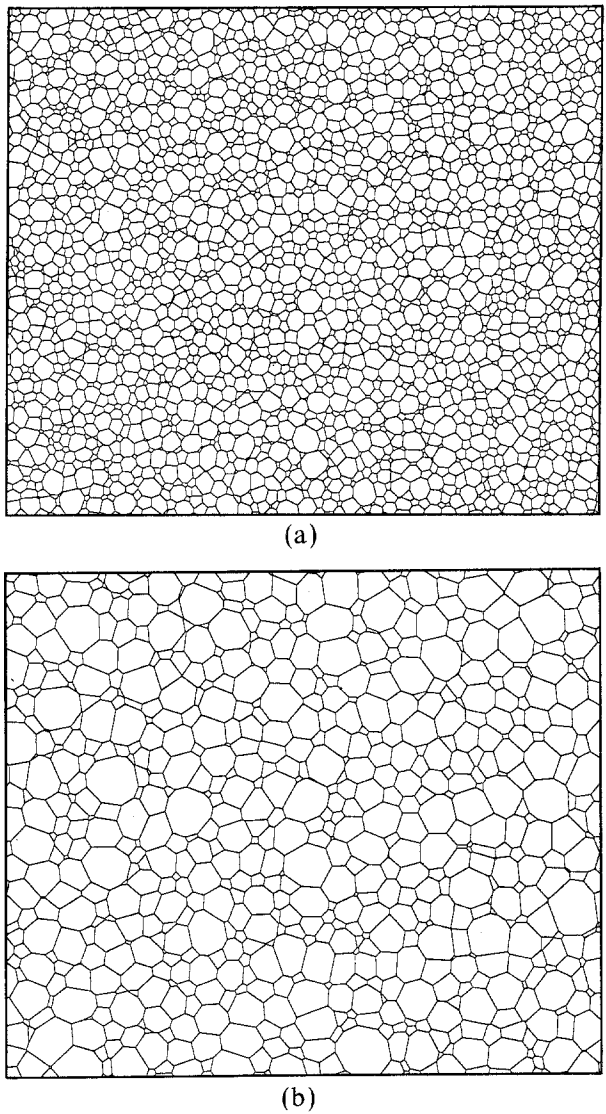

Fig. 3. Time evolution of the patterns for model II with $N(0)=48{,}000$: (a) $t=5.0$, (b) $t=20.0$, (c) $t=50.0$.

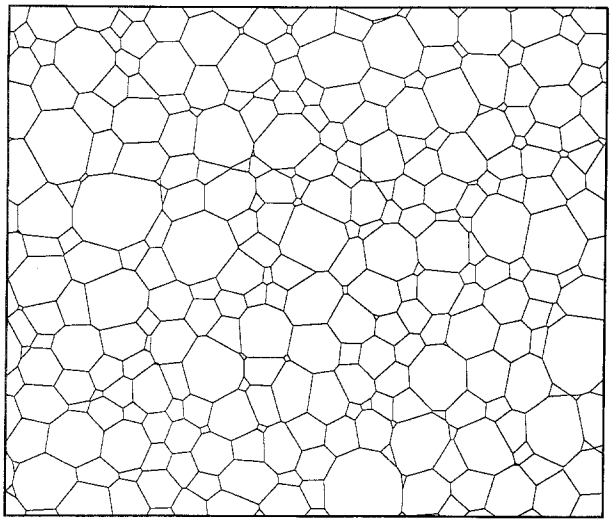

(c)

Fig. 3 (*continued*)

In Fig. 4 we show the simulation results for $\bar{A}(t)$ in four cases, model I, model II, the original model, and the original model without the correlation term, which is obtained by neglecting the correlation term $\mathbf{v}_j/2$ on the lhs in Eq. (2.4). Each result of $\bar{A}(t)$ is averaged over 10 runs in each case. For model I the time variable in Fig. 4 has been inversely transformed from τ to t with the use of Eq. (3.2). From this figure we can see that in each version $\bar{A}(t)$ grows linearly except in an initial transient regime. Therefore we obtain $\bar{R}(t) \sim t^{1/2}$ in the late stage. This result is easily understood by dimensional analysis of the equation of motion for vertices and agrees with those of the previous simulations.[6,7] The differences among the four versions result in different slopes of the linearity of $\bar{A}(t)$ with respect to t.

We study this by studing how the correlation term affects the velocity of a vertex in the original model. We get the distribution function of the angle θ between two velocities $\mathbf{v}_i$ and $\mathbf{v}_i'$, and the distribution function of the ratio of the absolute value of two velocities $|\mathbf{v}_i'|/|\mathbf{v}_i|$, where $\mathbf{v}_i'$ and $\mathbf{v}_i$ are the velocities of vertex i with and without the correlation term, respectively. The results are as follows. The average angle $\langle\theta\rangle$ is 0. The standard deviation of the angle θ is about 0.2 rad. The average ratio $\langle|\mathbf{v}_i'|/|\mathbf{v}_i|\rangle$ is about 0.71. The standard deviation of this ratio is about 0.16. Thus, because of the smallness of the standard deviations, we can roughly consider that the correlation term does not affect the direction of the velocity and only changes the absolute value by 0.71 time. From this, we can understand the

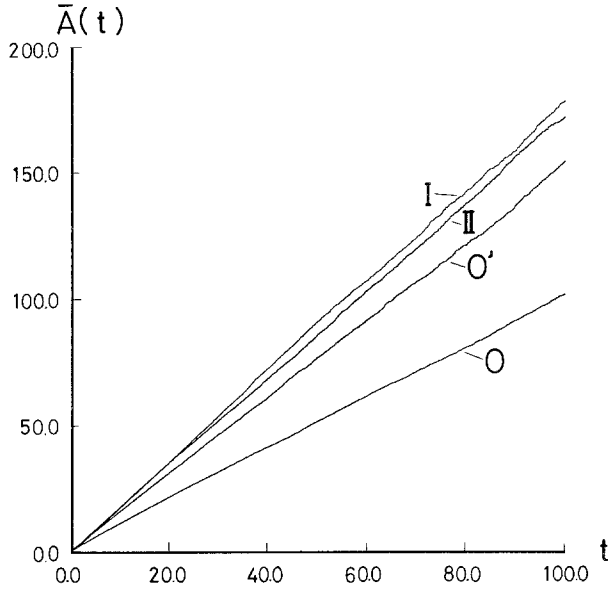

Fig. 4. Time dependence of the average cell area for model I (I), model II (II), the original model (O), and the original model without correlation term (O').

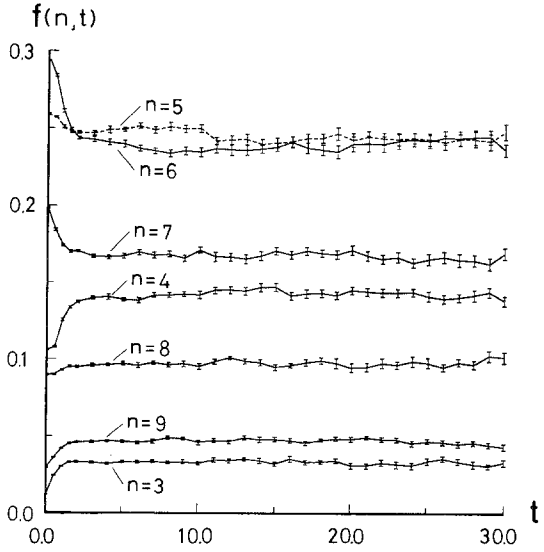

Fig. 5. Time variation of the distribution function of the number of cell edges for model II with $N(0) = 48{,}000$, averaged over 20 runs at each time.

ratio 0.66 of the slope of $\bar{A}(t)$ between the original models with and without the correlation term (see Section 5.4).

Next we examine the distribution function of the number of edges of a cell, which is denoted as $f(n, t)$ for n-sided cells at time t. In Fig. 5 we show the time variation of $f(n, t)$ for each n in model II, where the mean value of $f(n, t)$ over 20 runs at each time are plotted and the sizes of statistical errors are shown by the vertical bars. We can say from this figure that after $t \simeq 5.0$, $f(n, t)$ becomes approximately stationary for each n. Model I and the original model also yield the same behavior of $f(n, t)$ after the nearly same time $t \simeq 5.0$. In Fig. 5, the function $f(n, t)$ seems to be oscillating with small amplitudes of the same order of magnitude as the statistical error. However, this oscillation is not essential, as will be discussed below. We thus conclude that the distribution $f(n, t)$ is independent of time t in the scaling regime and can be written as

$$f(n, t) = f^*(n) \tag{4.2}$$

The small-amplitude oscillation of $f(n, t)$ mentioned above can be attributed to the effect of the finite size of the system. To show this, we present in Fig. 6 the simulation data for $f(n, t)$ obtained for two other cases, (a) $N(0) = 4800$ and 20 runs, and (b) $N(0) = 4800$ and 100 runs. Comparing the former result with that shown in Fig. 5, we see that the oscillation amplitude of $f(n, t)$ and the size of the statistical error simultaneously decrease with increasing system size. Furthermore, comparing the former result with the latter one, we find that the number of runs has the same effect on the oscillation and the statistical error as the system size. From this result, we conclude that the oscillation is a fluctuation effect which arises from the finiteness of the system size.

Next we study how the scaling function $f^*(n)$ depends on the system size. In practice, we examine systems with $N(0) = 4800$, 9600, 24,000, and 48,000, and repeat 20, 10, 10, and 20 runs, respectively. The scaling function $f^*(n)$ is determined by averaging $f(n, t)$ for $t \geqslant 5.0$ for each n. In Fig. 7 we show the graph of $f^*(n)$ vs. $N(0)$ for model II. From this figure we can see that the function $f^*(n)$ does not depend sensitively on the system size. This fact indicates that the correlation of cellular pattern is not long-ranged.

We examine the scaling behavior of the distribution of cell sizes $g(R, t)$, in which the cell size R is defined by the square root of the cell area. In the scaling regime the function $g(R, t)$ has the scaling property,

$$g(R, t) = [1/\bar{R}(t)]\, g^*(R/\bar{R}(t)) \tag{4.3}$$

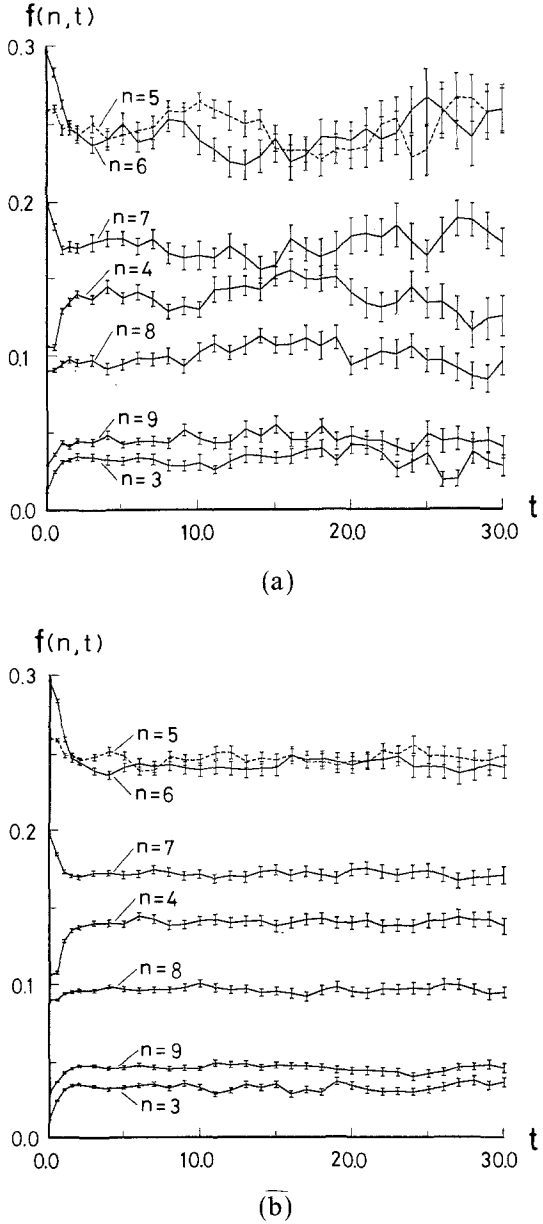

Fig. 6. Time variation of the distribution function of the number of cell edges for model II with $N(0) = 4800$, averaged over (a) 20 runs and (b) 100 runs at each time.

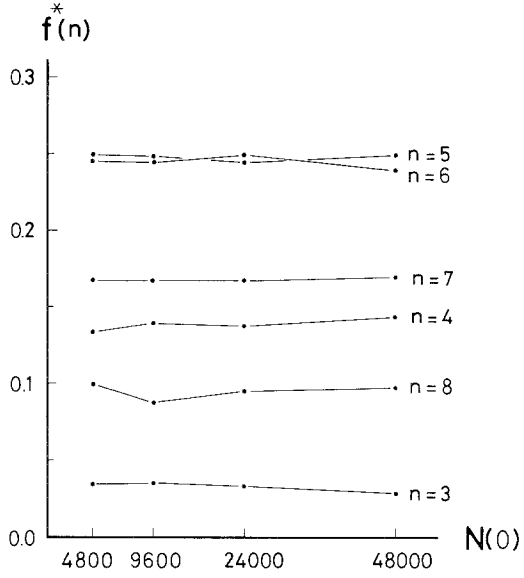

Fig. 7. System size dependence of the scaling function of the edge-number distribution for model II. The abscissa is the initial number of vertices.

where g^* is the scaling function. The function g^* is plotted in Fig. 8 at several different times for model II. This result shows that g^* is a function of the single variable $R/\bar{R}(t)$, as expressed in Eq. (4.3).

Lastly, we have studied whether or not the scaling behavior depends on the initial cellular pattern. We have examined it for the two kinds of

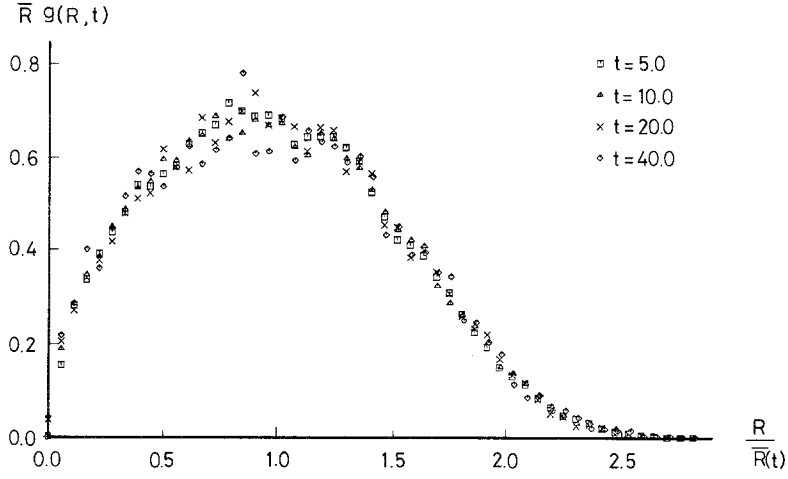

Fig. 8. Scaling function of the distribution of cell sizes for model II.

initial patterns shown in Figs. 2a and 2b. We obtained the same scaling behaviors in both cases. The only difference between the two cases is that the transient time region for the second pattern shown in Fig. 2b is longer than that for the first pattern shown in Fig. 2a. This is because the size distribution and the edge number distribution of the second pattern are sharper than those of the first.

5. ASYMPTOTIC BEHAVIOR IN THE SCALING REGIME

In this section we discuss several statistical quantities of the patterns in the scaling regime and compare scaling behaviors of the three versions of the vertex models.

5.1. Distribution of the Edge Number and the Cell Size

We have calculated the scaling functions for the distribution of the number of cell edges $f^*(n)$ defined by Eq. (4.2) and for that of cell sizes $g^*(R/\bar{R}(t))$ defined by Eq. (4.3) for each version of the vertex model. We plot the results for f^* in Fig. 9 and those for g^* in Fig. 10. These results are obtained by averaging over 20 independent runs and also over the scaling time regime for each version of the vertex models.

In each figure, the distribution becomes sharper gradually in the sequence of model I, model II, and the original model. The decrease of the distribution for small cells in this sequence can be understood by considering the shrinking rate of small cells. By comparing the friction coefficients of Eqs. (3.1), (3.3), and (3.7), we can say in a statistical sense that a cell with short sides shrinks faster in model II than in model I and in the original model than in model II. Taking account of the correlation between the size and the edge number of cells (see Section 5.3), we can say in the same sense that the distribution of few-sided cells decreases in the order of the models I, II, and the original. On the other hand, the decrease of the distribution for large cells in that sequence can be understood by considering the above-mentioned fact (i.e., the decrease for small size cells), and the correlation between the edge numbers of adjacent cells (see Section 5.2). The result for the correlation shown in Fig. 11 implies that a large cell has neighbors with small cell sizes on the average. Since the shrinking rate of a small cell becomes large in the same order of the model versions, the edge number of a large cell decreases faster on average in that order. Thus, the populations of cells with larger sizes or more edges may decrease in the same order.

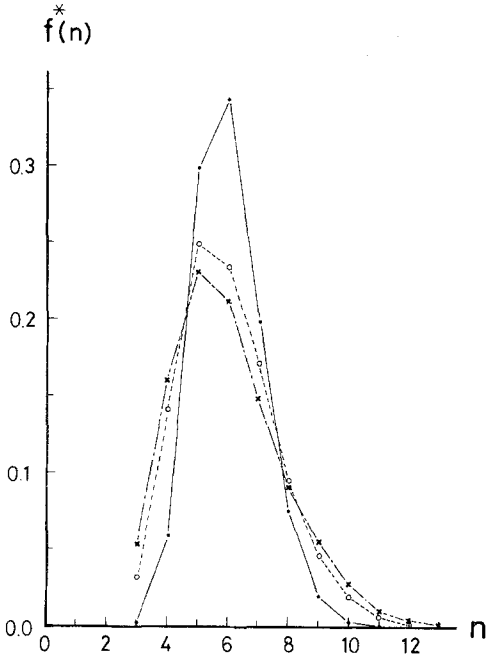

Fig. 9. Scaling functions of the distribution of the number of cell edges for three versions of the vertex model. Crosses, model I; open circles, model II; solid circles, the original model.

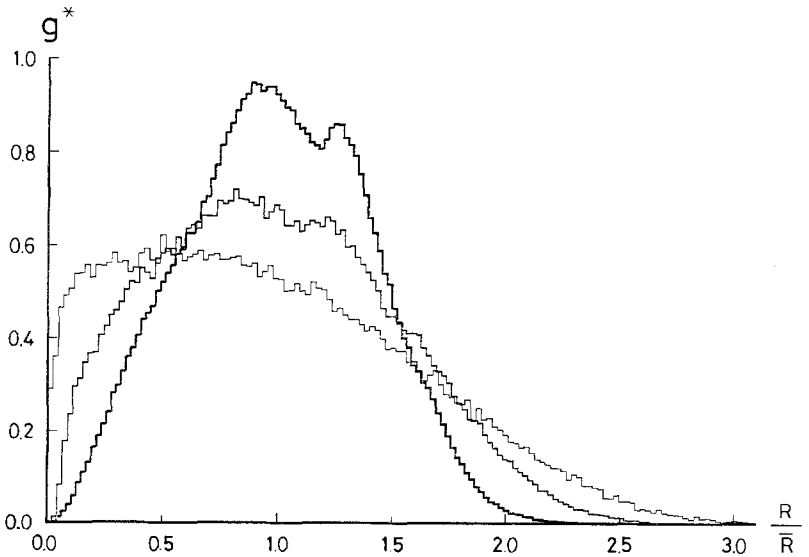

Fig. 10. Scaling function of the distribution of cell sizes for three versions of the vertex model. Thin line, model I; middle line, model II; thick line, the original model.

5.2. Correlation of the Edge Numbers of Neighboring Cells

The correlation between the edge numbers of adjacent cells is well known and is called the Aboav–Weaire hypothesis. This hypothesis states that the average edge number m_n of cells neighboring an n-sided cell is written as

$$m_n = K_1 + \frac{K_2}{n} \tag{5.1}$$

where K_1 and K_2 are positive constants. Recently Rivier estimated these constants from the two elementary processes which are the same as ours, and found that $K_1 = 5$ and $K_2 = 6 + \mu_2$, where $\mu_2 = \sum_n f(n)(n-6)^2$.[10] In Fig. 11 we plot our results observed in the scaling regime for each version of the vertex model. Equation (5.1) holds well in the vertex model except for small n ($n \lesssim 4$). The small discrepancy for small n is not yet understood. Hence we have calculated the coefficients K_1 and K_2 from the data for $n \geqslant 5$

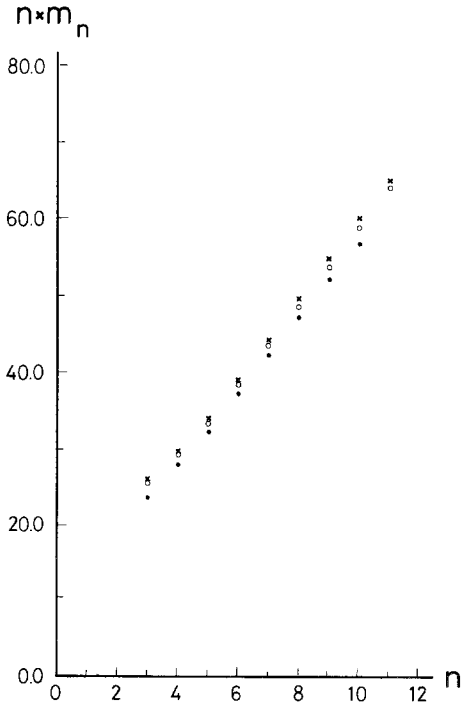

Fig. 11. Average number of edges of the first-neighbor cells adjacent to an n-sided cell $m_n(1)$ times n. Crosses, model I; open circles, model II; solid circles, the original model.

Table I. Coefficients K_1 and K_2 in the Aboav–Weaire Hypothesis (5.1), and the Variance of the Edge Number Distribution

	K_1	K_2	μ_2
Model I	5.23	7.71	3.40
Model II	5.14	7.57	2.66
Original model	4.91	7.80	1.29

for each version of the vertex model, and tabulate these coefficients and the variances μ_2 in Table I. Our results for the relation between the coefficient K_2 and the variance μ_2 disagree with Rivier's estimation.

Next, we have also examined the correlation of edge number between two cells separated by more than one cell. We denote the average edge number of the ith-neighbor cells adjacent to an n-sided cell by $m_n(i)$, i.e., $m_n(1) = m_n$. In Fig. 12 we show our results for $m_n(i)$ for several values of

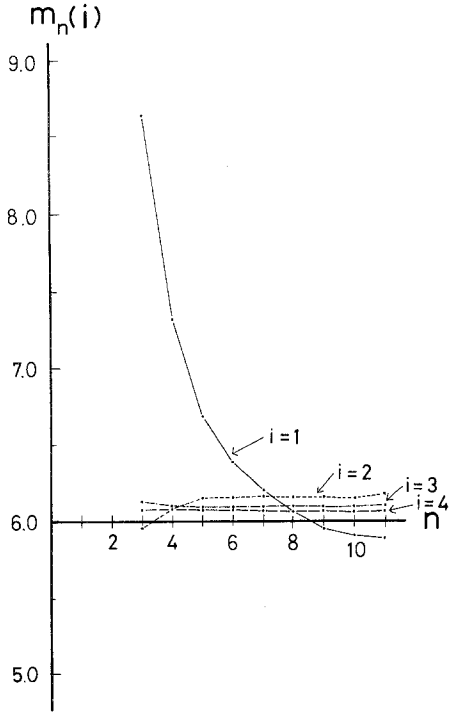

Fig. 12. Average number of edges of the ith-neighbor cells adjacent to an n-sided cell $m_n(i)$ for model II.

i, as observed in the scaling regime for model II. From this figure one can see that the correlation length of edge number is very short, i.e., nearly 1. This is consistent with the results of the previous section that the edge number distribution function does not depend sensitively on the system size. In Fig. 12, $m_n(i)$ are larger than 6.0 for almost every n for the second neighbors ($i=2$) and for every n for the more than third neighbors ($i \geqslant 3$). For $i \geqslant 2$, $m_n(i)$ takes an almost constant value for $n \geqslant 5$, which is larger than 6.0 and decreases with increasing i. This arises from the large variance of edge number distribution and also from the fact that many-sided cells contribute many times to $m_n(i)$. However, for larger i the contributions of many-sided cells are averaged out. Thus, $m_n(i)$ approaches 6.0 with increasing i for every n.

5.3. Correlation between the Edge Number and the Cell Size

It is known that a linear relationship exists between the average radius and the number of sides of a cell in a grain aggregate; this is called the perimeter hypothesis.[10] That is, the average radius or the average size $\bar{R}_n$ of n-sided cells is represented by

$$\bar{R}_n/\bar{R} = \alpha(n - n_0) \tag{5.2}$$

where α and n_0 are positive constants. In Fig. 13 we plot our simulation results for the average size $\bar{R}_n$ in the scaling regime for each version of the vertex model. From this figure we can see that there are discrepancies from the linear relationship for both cases with $n=3$ and $n \gtrsim 8$ for all versions of the vertex model. In particular, for $n \gtrsim 8$ the average cell size of the veretex model bends downward from the linear behavior as n increases.

Another relation, known as Lewis' hypothesis, states that the average area of n-sided cells is a linear function of its number of edges. That is, the average cell area $\bar{A}_n$ of n-sided cells is represented by

$$\bar{A}_n/\bar{A} = \beta(n - n_1) \tag{5.3}$$

where β and n_1 are constants.[10] This relation was originally proposed for biological cell tissues and afterward also for two-dimensional soap froths. We show in Fig. 14 our results for the average areas of n-sided cells normalized by the average area of cells, in the scaling regime for each version of the vertex model. We can see from this figure that the relation (5.3) is violated in the region of few-sided cells ($n \lesssim 5$), while it is obeyed in the region of many-sided cells ($n \gtrsim 6$). The violation of Lewis' hypothesis for few-sided cells has been reported experimentally in two-dimensional soap froths[1] and also in some numerical simulations.[11,12]

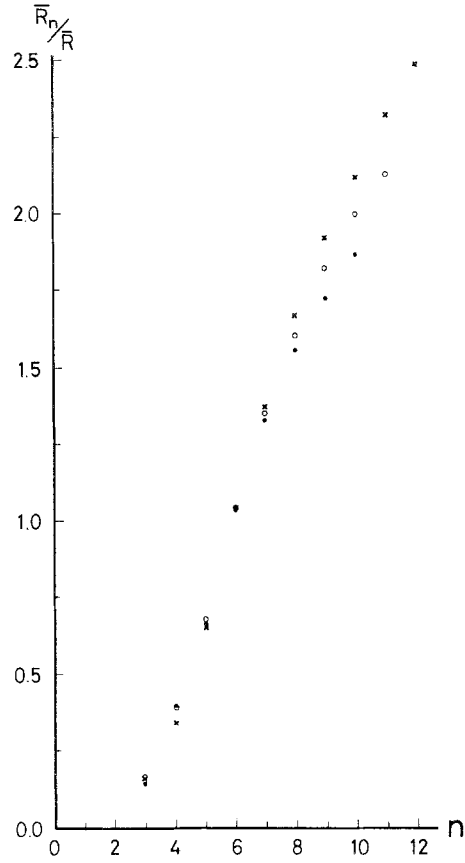

Fig. 13. Average radius of n-sided cells divided by the average radius of cells. All data are the mean values taken over 20 runs at $t = 10.0$ for each version of the vertex model. Crosses, model I; open circles, model II; solid circles, the original model.

5.4. Rate Equation for the Area of a Cell

For the vertex model we now examine the von Neumann–Mullins equation, which was derived for two-dimensional soap froths[13] and also for two-dimensional grain aggregates.[14] It states that the growth rate of a cell depends solely on its number of sides. That is, the area A_n of an n-sided cell varies according to the von Neumann–Mullins equation

$$\frac{dA_n}{dt} = \kappa(n-6) \tag{5.4}$$

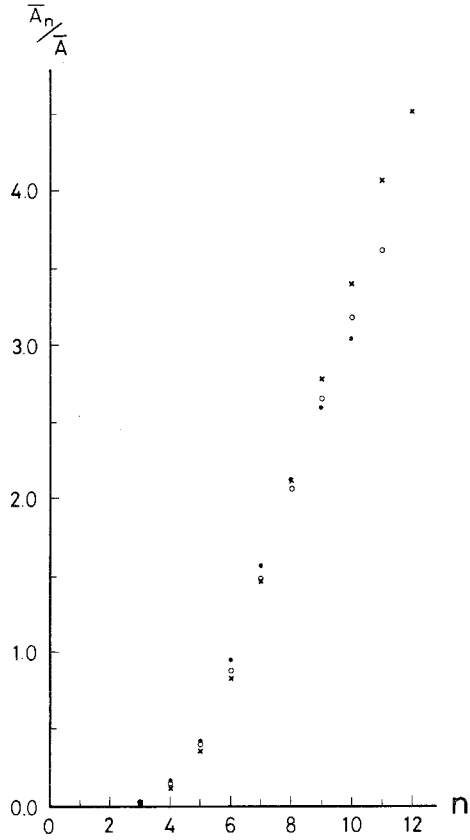

Fig. 14. Average area of n-sided cells divided by the average area of cells. All data are the mean values taken over 20 runs at $t = 10.0$ for each version of the vertex model. Crosses, model I; open circles, model II; solid circles, the original model.

where κ is a positive constant. This equation was derived from the following two assumptions: (1) curvature-driven interface dynamics where the velocity of a cell boundary is proportional to its mean curvature, and (2) the local equilibrium condition at the vertices that three cell boundaries meeting at a vertex form angles of 120°.

On the other hand, the vertex model does not satisfy these assumptions. However, this does not mean that Eq. (5.4) does not hold in the vertex model. It is a coarse-grained model in which vertices are replaced by effective ones with the finite size Δ, within the small region of which the local equilibrium condition is assumed to be satisfied by the original cell boundaries, and curved cell boundaries are replaced by straight effective ones with finite widths of order Δ. Thus, the constituents of the vertex

model, i.e., vertices and cell boundaries, are some averages of the original ones which retain only the minimal essentials. As a result, it is possible that the vertex model equation can include the effects of the two assumptions mentioned above implicitly and that Eq. (5.4) holds approximately on the average in the vertex model. In this case the parameter κ in Eq. (5.4) should be altered to a renormalized one, since the vertex model has poorer resolutions of space and time than the original interface model. On the other hand, it has been observed experimentally that the von Neumann–Mullins equation does not hold locally but statistically in two-dimensional soap froths.[1] Therefore, we examine below the growth rate of the average area $\bar{A}_n$ of n-sided cells in the scaling regime for each version of the vertex model.

Figure 15 shows the results for models I and II and the original model. In this figure we observe that the von Neumann–Mullins equation approximately holds for many-sided cells ($n \gtrsim 6$ for models I and II, and $n \gtrsim 4$ for the original model), while it fails for few-sided cells ($n \lesssim 5$ for the models I and II, and $n \sim 3$ for the original model). The deviations of the vertex model from the von Neumann–Mullins equation for few-sided cells arise from the fact that the difference of the straight cell boundary assumed in the vertex model from the curved one increases with decreasing number

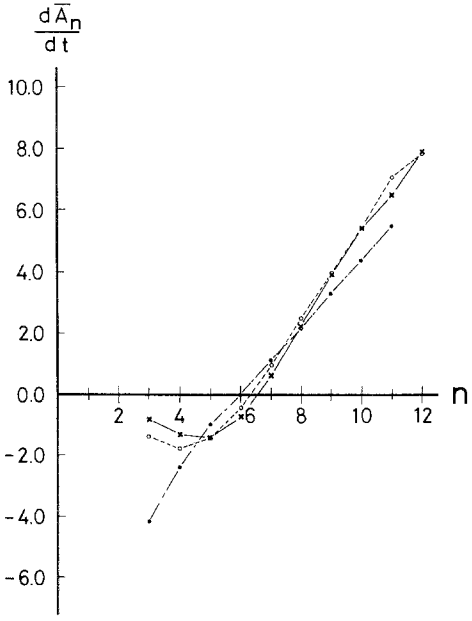

Fig. 15. Growth rates of the average area of n-sided cells. Crosses, model I, open circles, model II; solid circles, the original model.

of cell sides. A recent analysis of two-dimensional soap froth experiments[2] has also shown deviations from the von Neumann–Mullins equation, although the causes of deviations may not be the same. Further, we find that the growth rate for models I and II deviate upward from that of the original model for few-sided cells. This is due to the overestimation of the friction coefficient in the model I and model II equations.

We consider a special symmetric case analytically to see the meaning of the approximation in each version of the vertex model. We consider a regular n-sided cell. One of the three cell boundaries of each vertex of the cell emerges outward radially and symmetrically, which will be called the outer lines, and is connected to an outer vertex which is assumed to be fixed. Such a special symmetric case has been analyzed for comparison between the vertex model and the curvature-driven models of grain aggregates and soap froths in our previous paper.[9] Each vertex moves along its outer line due to the symmetric configuration. In this case Eq. (2.4) yields the outward velocity of a vertex given by, in the same units as in Section 3,

$$v_n = \frac{1 - 2\sin(\pi/n)}{[(2+c)/3]\, a_n \cos^2(\pi/n)} \tag{5.5}$$

where a_n is the length of an edge of the cell and $c = 0$ if the correlation term $(1/2)\,\mathbf{v}_j$ in Eq. (2.4) is neglected, while $c = 1$ if it is included. The latter corresponds to Eq. (4.22) in our previous paper.[9] In this equation the numerator and the denominator come from the line tension and the friction coefficient, respectively. The outer line gives no contribution to the friction coefficient because only the edges having finite projections upon the direction perpendicular to the velocity of the vertex can contribute to it. It has been shown in our previous paper[9] that Eq. (5.5) reasonably well describes the results of the curvature-driven models in the special symmetric case.

In this case the time derivative of the area A_n of the cell is given by

$$\frac{dA_n}{dt} = n v_n a_n \cos\frac{\pi}{n} \tag{5.6}$$

Substituting Eq. (5.5) into Eq. (5.6), we obtain

$$\frac{dA_n}{dt} = \frac{3}{2+c}\, n \frac{1 - 2\sin(\pi/n)}{\cos(\pi/n)} \tag{5.7}$$

This equation implies that the growth rate of the cell area depends solely on its number of edges, but not on its edge length. In Fig. 16 we plot the

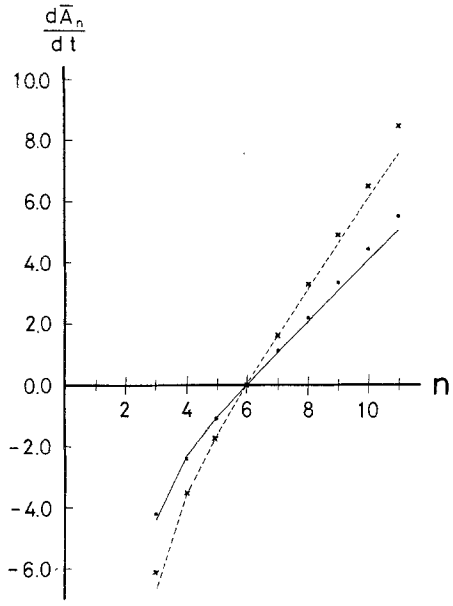

Fig. 16. Growth rate of the area of symmetric n-sided cells [solid line, $c=1$; dashed line, $c=0$ in Eq. (5.7)] and the average areas, where solid circles and crosses correspond to the vertex model with and without the correlation term, respectively.

growth rate given by Eq. (5.7) for $c=1$ by the solid line. The simulation results for the original model are plotted by the dots in the same figure. The agreement between them is excellent. This suggests that the special symmetric configuration of a cell considered above well describes the average behavior of the cell growth in the scaling regime. As seen in Fig. 16, Eq. (5.7) yields an approximate linear dependence of the growth rate on the number of cell edges for many-sided cells, as von Neumann–Mullins equation does. That is, expanding the rhs of Eq. (5.7) with respect to n, we have

$$\frac{dA_n}{dt} \simeq \frac{3}{2+c}\frac{\pi}{3}(n-6) \qquad \text{for} \quad n \sim 6 \tag{5.8}$$

$$\simeq \frac{3}{2+c}(n-2\pi) \qquad \text{for} \quad n \gg 1 \tag{5.9}$$

Equation (5.7) gives information on the effect of the correlation term $(1/2)\,\mathbf{v}_j$ in Eq. (2.4). If the correlation term is neglected, i.e., $c=0$ in Eq. (5.7), the growth rate of cell area becomes, in magnitude, 3/2 times as large as that in the case where it is included, while its n dependence is

unchanged. In Fig. 16 we plot the growth rate given by Eq. (5.7) for $c=0$ by the broken line. The simulation results for the original model without the correlation term is plotted by crosses in the same figure. Both are in good agreement, as in the case of $c=1$. The correlation term is also neglected in models I and II. Their difference from the original model without the correlation term resides in the difference in the friction coefficient. In models I and II three cell boundaries connected to a vertex contribute to its friction irrespective of its moving direction. Hence, the outer line contributes to the friction in the present special symmetric case. This is an overestimation of the friction coefficient, as mentioned previously. As a result, the absolute values of the velocity $|v_n|$ in these models are smaller than that in the case with $c=0$, and in turn the absolute values of the growth rate $|dA_n/dt|$ become small, as seen from Eq. (5.6). From this we can understand the behaviors of models I and II shown in Fig. 15, especially for $n=3$ and $n=4$.

6. CONCLUSION

We have studied two-dimensional domain growth by using the vertex model. This model contains the least amount of information which still permits the two kinds of elementary processes. Thus, it has enabled us to study the behaviors at late stages for systems with a large numbers of cells, and to confirm the scaling behavior, that is, the growth as 1/2 power in time of the average cell size, and the scaling properties of the distribution functions of the size and edge numbers of cells. However, the distributions of the original vertex model are not similar to those of the Potts model. Perhaps one of the reasons for this deviations is the assumption that the cell boundaries are straight in vertex models. However, we do not have a clear understanding as to why and how this assumption effects the distribution functions.

We have also studied several versions of the vertex model by making simplifying approximations on the equations of motion for vertices, and compared their scalng behaviors to each other. All versions yield the 1/2-power growth law for the average cell size. This is due to the fact that their equations of motion for vertices retain the same property with respect to dimensional analysis. On the other hand, distribution functions are different for each version and their differences arise from the differences in their friction coefficients. However, the correlations between the size and the edge number of a cell, the area and the edge number of a cell, and the edge numbers of neighboring cells are not so much different among different versions of the vertex model. This near absence of the differences is not fully understood.

Neither the perimeter hypothesis nor Lewis' hypothesis can be fitted on our simulation data over the whole observed range of the edge numbers of cells (from triangle to dodecagon) for the vertex model. The correlations of the edge number between neighboring cells are short-ranged in the vertex model. That is, the correlation is strong between nearest neighbors, while it approximately vanishes between more distant neighbors. The correlations between nearest neighbors are in accordance with the Aboav–Weaire hypothesis.

The vertex model treats the elementary processes of topological change exactly, but treats the equations of motion of vertices approximately. When we study the original cellular dynamics, we must improve on this aspect more accurately.

APPENDIX. CONSTRUCTION OF THE VORONOI CELL NETWORK

The Voronoi cell network is usually constructed as follows. First, one scatters nuclei at random in the plane simultaneously. Then one considers that nuclei grow isotropically with equal rates. As the nuclei grow, the domains which grow from different nuclei collide with each other, and new boundaries emerge between those domains. The cellular pattern formed after all the domains have completed their growth is the Voronoi cell network, as exemplified in Fig. 2a.

Now, from the method of construction mentioned above, we can see the following geometry of the Voronoi cell network. (1) The boundary is the perpendicular bisector of the straight line connecting two adjacent point nuclei. (2) The vertex which is the intersection of three boundaries is at equal distances from the point nuclei of three cells adjacent to the vertex, and there is no point nucleus within the circle passing through the three nuclei.

We can create this random cellular pattern on a computer as follows (see Fig. 17). First, we consider the plane in which point nuclei are scattered at random. We construct a cell in a computer around its point nucleus P in counterclockwise manner. If another point nucleus Q is nearest to the point nucleus P, then the cells P and Q have a common boundary. Next we search for a vertex A which is one of the endpoints of this boundary, which is also adjacent to the cell of a third point nucleus R. Since the cell P is constructed in counterclockwise manner, it is enough to search a candidate for R among point nuclei whose angle α in Fig. 17 lies between 0 and π. If we define the length h as in Fig. 17, then h has the smallest value for the point nucleus R and the vertex A which are chosen

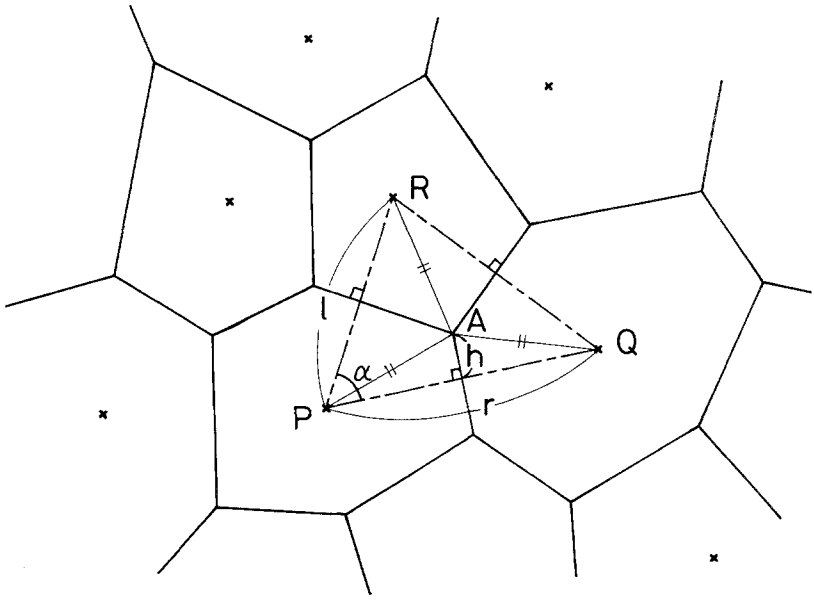

Fig. 17. Construction of the Voronoi cell network. The crosses denote the point nuclei of respective cells.

correctly. When we set the lengths $\overline{PQ} = r$ and $\overline{PR} = l$, the length h is given by

$$h = \frac{l - r\cos\alpha}{2\sin\alpha} \tag{A.1}$$

Consequently, the property of h mentioned above can be used in searching the correct point nucleus R and the corresponding vertex A.

Repeating the same procedure where the point nucleus Q is replaced by the point nucleus R, we can find still another vertex belonging to the cell P. Further repetitions of this process complete the construction of the cell P. A similar procedure produces other cells of the Voronoi cell pattern. In actual programming, it takes about 40 sec of CPU time to generate 24,000 cells on a FACOM M-780 computer.

ACKNOWLEDGMENTS

The authors are grateful to Dr. K. Sekimoto for a number of valuable discussions. This work was partially supported by the Scientific Research Fund of the Ministry of Education, Science and Culture.

It is a special pleasure for one of us (K.K.) to dedicate this article to Prof. E. G. D. Cohen. He owes a great deal to Eddie for his understanding of kinetic theory, which has been vital throughout his professional career.

REFERENCES

1. J. A. Glazier, S. P. Gross, and J. Stavans, *Phys. Rev. A* **36**:306 (1987).
2. J. Stavans and J. A. Glazier, *Phys. Rev. Lett.* **62**:1318 (1989).
3. G. S. Grest, M. P. Anderson, and D. J. Srolovitz, in *Proceedings NATO Conference on Time-Dependent Effects in Disordered Materials*, R. Pynn and T. Riste, eds. (Plenum, New York, 1988), and references cited therein.
4. D. Weaire and J. P. Kermode, *Philos. Mag. B* **50**:379 (1984).
5. C. W. J. Beenakker, *Phys. Rev. A* **37**:1697 (1988).
6. T. Nagai, K. Kawasaki, and K. Nakamura, *J. Phys. Soc. Japan* **57**:2221 (1988).
7. Y. Enomoto, K. Kawasaki, and T. Nagai, *Int. J. Mod. Phys. B* **3**:163 (1989).
8. K. Kawasaki, T. Nagai, and K. Nakashima, in *Proceedings 2nd Yukawa International Seminar on Coorperative Dynamics in Complex Physical Systems*, H. Takayama, ed. (Springer, Berlin, 1989), to be published.
9. K. Kawasaki, T. Nagai, and K. Nakashima, *Philos. Mag. B*, in press.
10. N. Rivier, *Philos. Mag. B* **52**:795 (1985), and references cited therein.
11. C. W. J. Beenakker, *Physica* **147A**:256 (1987).
12. M. Marder, *Phys. Rev. A* **36**:438 (1987).
13. J. von Neumann, in *Metal Interfaces*, C. Herring, ed. (American Society for Metals, Cleveland, Ohio, 1952), p. 108.
14. W. W. Mullins, *J. Appl. Phys.* **27**:900 (1956).